The Hall conductance, topological quantum phase transition and the Diophantine equation on honeycomb lattice

Masatoshi Sato,* Daijiro Tobe, and Mahito Kohmoto

The Institute for Solid State Physics, The University of Tokyo,

Kashiwanoha 5-1-5, Kashiwa, Chiba, 277-8581, Japan

(Dated: November 6, 2008)

Abstract

We consider a tight-binding model with the nearest neighbour hopping integrals on the honeycomb lattice in a magnetic field. Assuming one of the three hopping integrals, which we denote t_a, can take a different value from the two others, we study quantum phase structures controlled by the anisotropy of the honeycomb lattice. For weak and strong t_a regions, respectively, the Hall conductances are calculated algebraically by using the Diophantine equation. Except for a few specific gaps, we completely determine the Hall conductances in these two regions including those for subband gaps. In a weak magnetic field, it is found that the weak t_a region shows the unconventional quantization of the Hall conductance, $\sigma_{xy} = -(e^2/h)(2n+1)$, $(n = 0, \pm 1, \pm 2, \cdots)$, near the half-filling, while the strong t_a region shows only the conventional one, $\sigma_{xy} = -(e^2/h)n$, $(n = 0, 1, 2, \cdots)$. From topological nature of the Hall conductance, the existence of gap closing points and quantum phase transitions in the intermediate t_a region are concluded. We also study numerically the quantum phase structure in detail, and find that even when $t_a = 1$, namely in graphene case, the system is in the weak t_a phase except when the Fermi energy is located near the van Hove singularity or the lower and upper edges of the spectrum.

PACS numbers: Valid PACS appear here

*Electronic address: msato@issp.u-tokyo.ac.jp

I. INTRODUCTION

The purpose of this paper is to present some arguments for quantum Hall conductivity on the honeycomb lattice. Recently, quantized Hall effect is observed in graphene, and the Hall conductivity has been determined to be unconventionally quantized [1, 2],

$$\sigma_{xy} = -2(2n+1)\frac{e^2}{h}. \tag{1}$$

(The factor 2 comes from the spin degrees of freedom.) This unusual quantization is relevant when single particle physics dominates the behavior of the system [29], and it has been considered as a consequence of the existence of zero modes in graphene [3, 4, 5, 6]. In graphene, there exist zero modes in the absence of a magnetic field due to the honeycomb lattice structure, and the unconventional quantum Hall conductance (1) was explained by treating these zero modes as Dirac fermions [3, 4]. However, it is not trivial whether the Dirac fermion argument is true or not, because the Hall conductivity is given by an integral over whole Brillouin zone while the Dirac-fermion argument looks only the zero mode near the Fermi surface. Actually, it has been known that the logic of quantum Hall conductivity using the Dirac fermions is not correct in general [7]. Furthermore, numerical analyses for the tight-binding model of graphene have shown that the unconventional quantization persists up to the van Hove singularity where the Dirac fermion argument is no longer valid [8].

In this paper, we present an alternative explanation of the unconventional quantization by using the tight-binding model on the honeycomb lattice. For the tight-binding model on the honeycomb lattice, the energy spectrum in a magnetic field was studied in [9], and some numerical analyses for the Hall conductance have been done previously [8, 10, 11]. However no analytical study of the Hall conductance was presented systematically. Here we obtain the algebraic expression of the Hall conductances for almost all gaps including subband gaps, and explain why the unconventional quantum Hall effect (1) persists up to the van Hove singularity.

To obtain the algebraic expression of the Hall conductances, we study effects of anisotropy of the hopping parameters on the honeycomb lattice [10, 12, 13, 14]. For the square lattice, as suggested by Aubry-André duality[15], it is known that none of gaps closes when we change the ratio of the hopping parameters, t_x/t_y, and this facilitates the calculation of its Hall conductances [16]. For the honeycomb lattice, however, it will be found that gap closing

points appear since there is no duality. We present here a detailed study of the (topological) phase structures induced by the anisotropy of the hopping parameters on the honeycomb lattice, and determine its Hall conductances.

In the following, we describe the quantum Hall effect in terms of the Diophantine equation. For later convenience we present a brief derivation of the relation between the Hall conductance and the Diophantine equation [17]. First we use the Středa formula [18, 19] for the Hall conductance,

$$\sigma_{xy} = -e\frac{\partial \rho}{\partial B}, \tag{2}$$

where ρ is the electron density and the derivative is to be taken with the Fermi level fixed inside the gap. Then at the same time, the Hall conductance is written as [16, 20, 21]

$$\sigma_{xy} = -\frac{e^2}{h}t_r, \tag{3}$$

when the Fermi level is in the r-th gap from the bottom, where t_r is guaranteed to be an integer given by the Chern number. Combining them, we have

$$\frac{\partial \rho}{\partial B} = \frac{e}{h}t_r. \tag{4}$$

The energy gaps are stable under small perturbation and therefore persist under slight variation of B. Thus we obtain

$$\rho = \frac{\text{const.}}{v_0} + \frac{e}{h}Bt_r, \tag{5}$$

where v_0 is the area of a unit cell. (Here const./v_0 is a constant of integration.) When the flux per unit cell is $\Phi = p/q$ (in units of h/e) where p and q are co-prime integers and $q > 0$, the area of the magnetic Brillouin zone is $((2\pi)^2/v_0 q)$, and the density of electrons in a single band is given by $(1/v_0 q)$. Thus, when there are r bands below the Fermi energy, the density of electrons is

$$\rho = \frac{r}{v_0 q}. \tag{6}$$

Then (5) is rewritten as

$$r = \text{const.} \times q + pt_r. \tag{7}$$

In this equation, r, p and t_r are integers, thus const. $\times$ q must be an integer. However, since const. is independent of q and q can change when the magnetic field is varied without making a point of contact, then const. itself must be an integer s_r. Thus we have

$$r = qs_r + pt_r, \tag{8}$$

which is the Diophantine equation.

The plan of the remainder of the paper is as follows. In Sec.II, we explain the tight-binding model on the honeycomb lattice briefly. An anisotropic hopping parameter t_a is introduced in the tight-binding model. In Sec.III, the weak t_a limit is studied. It is shown that the Hall conductances for almost all gaps including subband ones are determined algebraically by using the Diophantine equation. Furthermore, in a weak magnetic field, the unconventional Hall effect (1) is found to hold for visible gaps. We study the strong t_a limit in Sec.IV. In this limit, our model on the honeycomb lattice is shown to reduce to a pair of the tight-binding models on the square lattice. Using this result, we establish an algebraic rule to determine the Hall conductances in the strong t_a limit. It is found that the algebraic rule in the strong t_a limit is different from one in the weak t_a limit. As a result, only conventional quantization of the Hall conductance is obtained in this limit. From the differences of the Hall conductances between the two limits, the existence of the gap closing points and topological quantum phase transitions in the intermediate t_a region are concluded. In Sec.V, we study the topological quantum phase transitions in the intermediate t_a region in detail. The existence of the gap closing points is confirmed numerically. In addition, we will find that for some gaps near the van Hove singularity at $t_a = 1$ or on the lower and upper edges of the spectrum unexpected topological quantum phase transitions occur due to accumulation of gaps in a weak magnetic field. In Sec.VI, we apply our results to graphene where t_a is given by 1 and determine its Hall conductance. The unconventional quantization of the Hall conductance is obtained from our results. It is also explained naturally why it persists up to the van Hove singularity. In Sec.VI, we also examine the edge states of graphene in a weak magnetic field, in order to confirm our results using the bulk-edge correspondence. Finally, in Sec.VII, we will summarize our results.

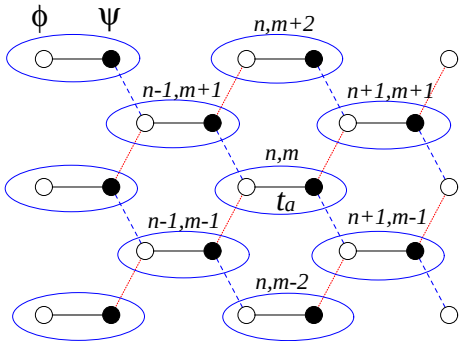

FIG. 1: The honeycomb lattice. Closed and open circles shows sublattice A and B, respectively. t_a is the hopping integral of the horizontal bond.

II. MODEL

Let us consider the tight-binding model on the honeycomb lattice with the nearest neighbour hopping in a magnetic field. See Fig.1. Denote wave functions on sublattices A and B as $\psi_{n,m}$ and $\phi_{n,m}$, respectively, then the tight-binding model is given by

$$\begin{aligned} -\phi_{n+1,m-1} - \phi_{n+1,m+1} - t_a e^{-i\pi\Phi m}\phi_{n,m} + \xi\psi_{n,m} &= E\psi_{n,m}, \\ -\psi_{n-1,m+1} - \psi_{n-1,m-1} - t_a e^{i\pi\Phi m}\psi_{n,m} - \xi\phi_{n,m} &= E\phi_{n,m}, \end{aligned} \tag{9}$$

where a magnetic flux through a unit hexagon is given by Φ, the hopping integrals of the horizontal bonds are t_a and those for the other bonds are 1. Here we have introduced potentials ξ on sublattice A and $-\xi$ on sublattice B to remove a subtle singularity at $E = 0$. We take $\xi \to 0$ in the final stage of analysis. For simplicity we neglect the spin degrees of freedom in the following.

III. WEAK t_a PHASE

In this section, we study the weak coupling limit of the horizontal bond $t_a \ll 1$. Using the perturbation theory, we derive the Diophantine equation and provide a general rule to determine the Hall conductances. We also find that the unconventional quantization (1) holds in a weak magnetic field.

A. weak t_a perturbation

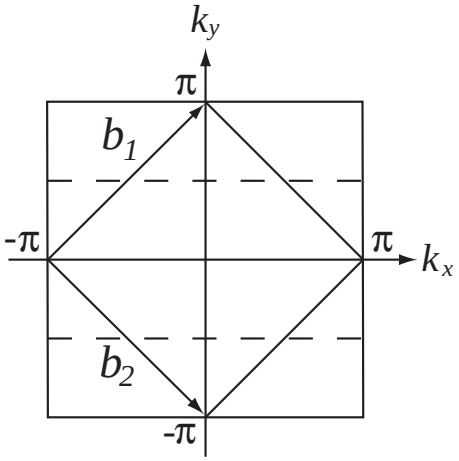

FIG. 2: The first and the second Brillouin zones for $\Phi = 0$ in the momentum space defined by (10). The primitive vectors are $\boldsymbol{a}_1 = (1, 1)$ and $\boldsymbol{a}_2 = (1, -1)$ in the space of (n, m), so the generators of the reciprocal lattice are $\boldsymbol{b}_1 = \pi(1, 1)$ and $\boldsymbol{b}_2 = \pi(1, -1)$.

Let us consider (9) in the momentum space. By performing the Fourier transformation of $\psi_{n,m}$ and $\phi_{n,m}$,

$$\begin{aligned} \psi_{n,m} &= \sum_{k_x,k_y} e^{ik_x n + ik_y m} u(\boldsymbol{k}), \\ \phi_{n,m} &= \sum_{k_x,k_y} e^{ik_x n + ik_y m} v(\boldsymbol{k}), \end{aligned} \tag{10}$$

(9) becomes

$$h(\boldsymbol{k}) \begin{bmatrix} u(k_x, k_y) \\ v(k_x, k_y) \end{bmatrix} - t_a \sigma_+ \begin{bmatrix} u(k_x, k_y + \pi\Phi) \\ v(k_x, k_y + \pi\Phi) \end{bmatrix} - t_a \sigma_- \begin{bmatrix} u(k_x, k_y - \pi\Phi) \\ v(k_x, k_y - \pi\Phi) \end{bmatrix} = E \begin{bmatrix} u(\boldsymbol{k}) \\ v(\boldsymbol{k}) \end{bmatrix}, \tag{11}$$

where $h(\boldsymbol{k})$ and $\sigma_\pm$ are given by

$$h(\boldsymbol{k}) = \begin{bmatrix} \xi & \Delta^{(0)}(\boldsymbol{k}) \\ \Delta^{(0)*}(\boldsymbol{k}) & -\xi \end{bmatrix}, \quad \Delta^{(0)}(\boldsymbol{k}) = -2e^{ik_x} \cos k_y, \tag{12}$$

and

$$\sigma_+ = \begin{bmatrix} 0 & 1 \\ 0 & 0 \end{bmatrix}, \quad \sigma_- = \begin{bmatrix} 0 & 0 \\ 1 & 0 \end{bmatrix}. \tag{13}$$

When $t_a = 0$, (11) reduces to

$$h(\boldsymbol{k}) \begin{bmatrix} u^{(0)}(\boldsymbol{k}) \\ v^{(0)}(\boldsymbol{k}) \end{bmatrix} = E \begin{bmatrix} u^{(0)}(\boldsymbol{k}) \\ v^{(0)}(\boldsymbol{k}) \end{bmatrix}, \tag{14}$$

then the energies E are found to be

$$E = \pm\sqrt{\xi^2 + 4\cos^2 k_y} (\equiv \pm E^{(0)}(k_y)), \tag{15}$$

and the eigen vector with the positive energy, $E = E^{(0)}(k_y)$, is

$$\begin{bmatrix} u_+^{(0)}(\boldsymbol{k}) \\ v_+^{(0)}(\boldsymbol{k}) \end{bmatrix} = \frac{1}{\sqrt{2E^{(0)}(k_y)(\xi + E^{(0)}(k_y))}} \begin{bmatrix} \xi + E^{(0)}(k_y) \\ \Delta^{(0)*}(\boldsymbol{k}) \end{bmatrix}, \tag{16}$$

and that with the negative one, $E = -E^{(0)}(k_y)$, is

$$\begin{bmatrix} u_-^{(0)}(\boldsymbol{k}) \\ v_-^{(0)}(\boldsymbol{k}) \end{bmatrix} = \frac{1}{\sqrt{2E^{(0)}(k_y)(\xi + E^{(0)}(k_y))}} \begin{bmatrix} -\Delta^{(0)}(\boldsymbol{k}) \\ \xi + E^{(0)}(k_y) \end{bmatrix}. \tag{17}$$

Here the staggered potential ξ removes singularities in the energies, $\pm E^{(0)}(k_y)$, and the eigen vectors at $k_y = \pm\pi/2$. It also remedies the singularity of $\boldsymbol{A}(\boldsymbol{k})$ in (41) at $k_y = \pm\pi/2$. To solve (11) in perturbative expansions in powers of t_a, it is convenient to take the basis $(u(\boldsymbol{k}), v(\boldsymbol{k}))$ as

$$\begin{bmatrix} u(\boldsymbol{k}) \\ v(\boldsymbol{k}) \end{bmatrix} = \alpha(\boldsymbol{k}) \begin{bmatrix} u_+^{(0)}(\boldsymbol{k}) \\ v_+^{(0)}(\boldsymbol{k}) \end{bmatrix} + \beta(\boldsymbol{k}) \begin{bmatrix} u_-^{(0)}(\boldsymbol{k}) \\ v_-^{(0)}(\boldsymbol{k}) \end{bmatrix}. \tag{18}$$

Substituting this into (11) and multiplying $(u_+^{(0)*}(\boldsymbol{k}), v_+^{(0)*}(\boldsymbol{k}))$ to the both sides, we obtain

$$\begin{aligned}
&\left(E - E^{(0)}(k_y^0 + \pi\Phi m)\right) \alpha_m(k_x, k_y^0) = \\
&-t_a \left[u_+^{(0)*}(k_x, k_y^0 + \pi\Phi m) v_+^{(0)}(k_x, k_y^0 + \pi\Phi(m+1))\right] \alpha_{m+1}(k_x, k_y^0) \\
&-t_a \left[u_+^{(0)*}(k_x, k_y^0 + \pi\Phi m) v_-^{(0)}(k_x, k_y^0 + \pi\Phi(m+1))\right] \beta_{m+1}(k_x, k_y^0) \\
&-t_a \left[v_+^{(0)*}(k_x, k_y^0 + \pi\Phi m) u_+^{(0)}(k_x, k_y^0 + \pi\Phi(m-1))\right] \alpha_{m-1}(k_x, k_y^0) \\
&-t_a \left[v_+^{(0)*}(k_x, k_y^0 + \pi\Phi m) u_-^{(0)}(k_x, k_y^0 + \pi\Phi(m-1))\right] \beta_{m-1}(k_x, k_y^0),
\end{aligned} \tag{19}$$

where $\alpha_m(k_x, k_y^0)$ and $\beta_m(k_x, k_y^0)$ are defined as

$$\alpha_m(k_x, k_y^0) = \alpha(k_x, k_y^0 + \pi\Phi m), \quad \beta_m(k_x, k_y^0) = \beta(k_x, k_y^0 + \pi\Phi m), \tag{20}$$

and k_y^0 satisfies $0 \leq k_y^0 < 2\pi/q$. Here we have used the normalization conditions of the functions $(u_+^{(0)}(\boldsymbol{k}), v_+^{(0)}(\boldsymbol{k}))$ and $(u_-^{(0)}(\boldsymbol{k}), v_-^{(0)}(\boldsymbol{k}))$. In a similar manner, we also have

$$
\begin{aligned}
&\left(E + E^{(0)}(k_y^0 + \pi\Phi m)\right)\beta_m(k_x, k_y^0) = \\
&-t_a\left[u_-^{(0)*}(k_x, k_y^0 + \pi\Phi m)v_+^{(0)}(k_x, k_y^0 + \pi\Phi(m+1))\right]\alpha_{m+1}(k_x, k_y^0) \\
&-t_a\left[u_-^{(0)*}(k_x, k_y^0 + \pi\Phi m)v_-^{(0)}(k_x, k_y^0 + \pi\Phi(m+1))\right]\beta_{m+1}(k_x, k_y^0) \\
&-t_a\left[v_-^{(0)*}(k_x, k_y^0 + \pi\Phi m)u_+^{(0)}(k_x, k_y^0 + \pi\Phi(m-1))\right]\alpha_{m-1}(k_x, k_y^0) \\
&-t_a\left[v_-^{(0)*}(k_x, k_y^0 + \pi\Phi m)u_-^{(0)}(k_x, k_y^0 + \pi\Phi(m-1))\right]\beta_{m-1}(k_x, k_y^0).
\end{aligned} \tag{21}
$$

When $t_a = 0$, these equations reduce to

$$
\begin{aligned}
(E - E^{(0)}(k_y^0 + \pi\Phi m))\alpha_m(k_x, k_y^0) = 0, \\
(E + E^{(0)}(k_y^0 + \pi\Phi m))\beta_m(k_x, k_y^0) = 0,
\end{aligned} \tag{22}
$$

and the unperturbed solutions are given by

$$
E = E^{(0)}(k_y^0 + \pi\Phi m), \quad \alpha_m(k_x, k_y^0) = 1, \quad \beta_m(k_x, k_y^0) = 0, \tag{23}
$$

and

$$
E = -E^{(0)}(k_y^0 + \pi\Phi m), \quad \alpha_m(k_x, k_y^0) = 0, \quad \beta_m(k_x, k_y^0) = 1, \tag{24}
$$

which reproduce (16) and (17), respectively. In the new basis, $\alpha(\boldsymbol{k})$ and $\beta(\boldsymbol{k})$ describe the upper ($E > 0$) and lower ($E < 0$) bands, respectively. The energy spectrum for $t_a = 0$ is shown in Fig.3.

In (19) and (21), the terms proportional to t_a give couplings between the momenta k_y and $k_y \pm \pi\Phi$. So, if we put $\Phi = p/q$ with co-prime integers p and q ($q > 0$), then in general gaps open when $E^{(0)}(k_y) = E^{(0)}(k_y')$ with

$$
k_y = k_y' + \pi\left(\frac{p}{q}\right)t, \quad k_y = -k_y' + \pi s. \tag{25}
$$

Here s is an integer, and k_y and k_y' couple by $|t|$th-order perturbation. The size of the gap is an order of $t_a^{|t|}$. If s is chosen appropriately, k_y is put between 0 and π and k_y for the r-th gap from the bottom can be chosen as

$$
k_y = \left(\frac{r}{2q}\right)\pi, \tag{26}
$$

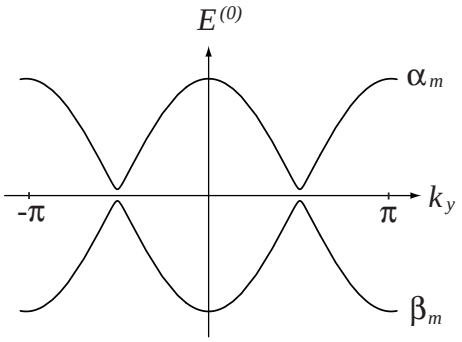

FIG. 3: The energy spectrum for $t_a = 0$. The upper band and lower one correspond to the eigen state with $\alpha_m = 1$ and one with $\beta_m = 1$, respectively. We show the case of $\xi = 0.05$.

where r is an integer with $1 \leq r \leq 2q-1$. (Gaps with $1 \leq r \leq q-1$ open in the lower band ($E < 0$), and those with $q+1 \leq r \leq 2q-1$ open in the upper band ($E > 0$). A gap at $E = 0$ corresponds to $r = q$, but it closes when $\xi \to 0$ for a weak t_a.) Eliminating k_y and k'_y from (25) and (26), we have the Diophantine equation

$$r = qs_r + pt_r, \tag{27}$$

where we have written the subscript r since t and s depend on r implicitly as a solution of (27).

We can also derive the formula (3) in the perturbation theory. For brevity, we derive it only for gaps in the upper band ($E > 0$). The same formula can be obtained for gaps in the lower band ($E < 0$) in a similar manner. The wave function in the upper band ($E > 0$) is simply given by

$$\begin{bmatrix} u(k_x, k_y^0) \\ v(k_x, k_y^0) \end{bmatrix} = \alpha_m(k_x, k_y^0) \begin{bmatrix} u_+^{(0)}(k_x, k_y^0 + \pi\phi m) \\ u_-^{(0)}(k_x, k_y^0 + \pi\phi m) \end{bmatrix} + \alpha_{m'}(k_x, k_y^0) \begin{bmatrix} u_+^{(0)}(k_x, k_y^0 + \pi\phi m') \\ u_-^{(0)}(k_x, k_y^0 + \pi\phi m') \end{bmatrix} \tag{28}$$

where $m = m' + t$ and we take $0 \leq k_y^0 < \pi/q$. The gaps are at $k_y^0 = 0$ and $\pi/2q$. Write $\alpha_m = a$ and $\alpha_{m'} = b$, then an effective Schrödinger equation is given by

$$\begin{bmatrix} \epsilon & \eta e^{ik_x t} \\ \eta e^{-ik_x t} & -\epsilon \end{bmatrix} \begin{bmatrix} a \\ b \end{bmatrix} = E \begin{bmatrix} a \\ b \end{bmatrix}, \tag{29}$$

where ϵ and E are measured from the middle of the gap, namely

$$E = E^{(0)}(k_y^0 + \pi\phi m), \tag{30}$$

and $k_y^0 = 0$ for even r or $\pi/2q$ for odd r. Here the k_x-dependence of the off diagonal elements of the matrix in (29) is determined by (16), (17) and (19), and the parameter η is a real number and of the order of $t_a^{|t|}$. The solutions of (29) are

$$E_+ = \sqrt{\epsilon^2 + \eta^2},$$
$$\begin{bmatrix} a_+ \\ b_+ \end{bmatrix} = \frac{1}{\sqrt{2E_+(E_+ - \epsilon)}} \begin{bmatrix} \eta \\ (E_+ - \epsilon)e^{-ik_x t} \end{bmatrix}, \tag{31}$$

and

$$E_- = -\sqrt{\epsilon^2 + \eta^2},$$
$$\begin{bmatrix} a_- \\ b_- \end{bmatrix} = \frac{1}{\sqrt{2E_-(E_- - \epsilon)}} \begin{bmatrix} \eta \\ (E_- - \epsilon)e^{-ik_x t} \end{bmatrix}. \tag{32}$$

When $\epsilon/|\eta| \to \infty$, these solutions behave as

$$\begin{bmatrix} a_+ \\ b_+ \end{bmatrix} \to \begin{bmatrix} \mathrm{sgn}\eta \\ 0 \end{bmatrix}, \quad \begin{bmatrix} a_- \\ b_- \end{bmatrix} \to \begin{bmatrix} 0 \\ -e^{-ik_x t} \end{bmatrix}, \tag{33}$$

and when $\epsilon/|\eta| \to -\infty$,

$$\begin{bmatrix} a_+ \\ b_+ \end{bmatrix} \to \begin{bmatrix} 0 \\ e^{-ik_x t} \end{bmatrix}, \quad \begin{bmatrix} a_- \\ b_- \end{bmatrix} \to \begin{bmatrix} \mathrm{sgn}\eta \\ 0 \end{bmatrix}. \tag{34}$$

For the upper edges of r-th band, we take the solution (32) with $t = t_r$. The asymptotic behaviors (33) and (34) imply that as k_y^0 passes 0 (for even r) or $\pi/2q$ (for odd r), the wave function changes from

$$\begin{bmatrix} u(k_x, k_y^0) \\ v(k_x, k_y^0) \end{bmatrix}_- = \mathrm{sgn}\eta \begin{bmatrix} u_+^{(0)}(k_x, k_y^0 + \pi\phi m) \\ u_+^{(0)}(k_x, k_y^0 + \pi\phi m) \end{bmatrix} \tag{35}$$

to

$$\begin{bmatrix} u(k_x, k_y^0) \\ v(k_x, k_y^0) \end{bmatrix}_- = -e^{-ik_x t_r} \begin{bmatrix} u_+^{(0)}(k_x, k_y^0 + \pi\phi m') \\ u_+^{(0)}(k_x, k_y^0 + \pi\phi m') \end{bmatrix}. \tag{36}$$

And for the lower edge of r-th band, we take the solution (31) with $t = t_{r-1}$, then we have asymptotic behaviors of the wave function in a similar manner. On the overlap in the center

of the band, these wave functions are related to each other by transition functions. See Fig.4. On the overlap I in Fig.4, the wave function (35) is identified with

$$\begin{bmatrix} u(k_x, k_y^0) \\ v(k_x, k_y^0) \end{bmatrix}_+ = \mathrm{sgn}\eta \begin{bmatrix} u_+^{(0)}(k_x, k_y^0 + \pi\phi m) \\ u_+^{(0)}(k_x, k_y^0 + \pi\phi m) \end{bmatrix}, \tag{37}$$

by a trivial transition function, $e^{i\theta} = 1$, and on the overlap II, (36) is identified with

$$\begin{bmatrix} u(k_x, k_y^0) \\ v(k_x, k_y^0) \end{bmatrix}_+ = e^{-ik_x t_{r-1}} \begin{bmatrix} u_+^{(0)}(k_x, k_y^0 + \pi\phi m') \\ u_+^{(0)}(k_x, k_y^0 + \pi\phi m') \end{bmatrix}, \tag{38}$$

by the transition function

$$e^{i\theta(k_x)} = -e^{ik_x(t_r - t_{r-1})}. \tag{39}$$

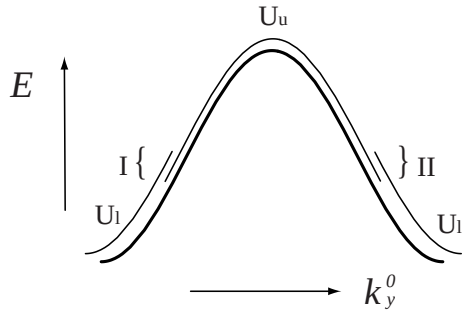

FIG. 4: An upper edge U_u and a lower one U_l of a band. They overlaps in the regions I and II.

Now let us calculate the contribution of the r-th band to the Hall conductance,

$$\sigma_{xy}^{(r)} = -\frac{e^2}{h}\frac{1}{2\pi}\int\int dk_x dk_y^0 (\nabla_{\boldsymbol{k}} \times \boldsymbol{A}(\boldsymbol{k}))_z. \tag{40}$$

Here the integration of (40) is performed on the first magnetic Brillouin zone, and $\boldsymbol{A}(\boldsymbol{k})$ is defined as

$$\boldsymbol{A}(\boldsymbol{k}) = -i[u^*(\boldsymbol{k})\nabla_{\boldsymbol{k}} u(\boldsymbol{k}) + v^*(\boldsymbol{k})\nabla_{\boldsymbol{k}} v(\boldsymbol{k})], \tag{41}$$

where $(u(\boldsymbol{k}), v(\boldsymbol{k}))$ is the wave function for the r-th band constructed above. For the present purpose, it is convenient to consider the rectangle region given by $-\pi \leq k_x < \pi$ and $0 \leq k_y^0 < 2\pi/q$, which is equivalent to a pair of the first magnetic Brillouin zone. Performing the integral (40) in this region and dividing it by 2, we have

$$\sigma_{xy}^{(r)} = -\frac{e^2}{h}\frac{1}{4\pi}\int_{-\pi}^{\pi} dk_x \int_0^{2\pi/q} dk_y^0 (\nabla_{\boldsymbol{k}} \times \boldsymbol{A}(\boldsymbol{k}))_z. \tag{42}$$

From the Stokes theorem, one can show that only the transition function (39) in the center of the band contributes to this integral. Thus we obtain

$$\sigma_{xy}^{(r)} = -\frac{e^2}{h}\frac{1}{4\pi}\int_{-\pi}^{\pi} dk_x \partial_x \theta(k_x) \times 2 = -\frac{e^2}{h}(t_r - t_{r-1}). \tag{43}$$

(The factor 2 arises because we have the transition function (39) twice in the integral region of (42).) When the Fermi surface is in the r-th gap from the bottom, we have the formula (3),

$$\sigma_{xy} = \sum_{r'=1}^{r} \sigma_{xy}^{(r')} = -\frac{e^2}{h} t_r. \tag{44}$$

B. Hall conductance and the Diophantine equation

Let us now determine the Hall conductance. As we showed above, the Hall conductance in units of $-e^2/h$, namely t_r, satisfies the Diophantine equation. By combining with the perturbation theory, the Diophantine equation enables us to determine the Hall conductance algebraically.

Before giving a rule to determine the Hall conductance, we briefly summarize properties of the Diophantine equation which we shall use later. First, the Diophantine equation has an infinite number of solutions: If we have a solution (s_r, t_r) for a given r, then $(s_r - lp, t_r + lq)$ for any integer l is also a solution. Second, the minimal value of $|t_r|$ among the solutions satisfies $|t_r| \leq q/2$. We denote a solution with the minimal $|t_r|$ by (s_r^0, t_r^0). Third, except when q is an even integer and $|t_r| = q/2$, (s_r^0, t_r^0) is uniquely determined. When $|t_r| = q/2$, we have two solutions: $t_r^0 = \pm q/2$.

As we denoted in Sec.III A, $|t_r|$ is an order of the perturbation. So one naively expect that the size of the rth gap from the bottom and its Hall conductance are given by its minimal value t_r^0. But this is not always correct. The reason why is that if an intermediate state in the $|t_r^0|$th order perturbation has the momentum $\boldsymbol{k}$ with $\Delta^{(0)}(\boldsymbol{k}) = 0$, (namely $\boldsymbol{k}$ with $k_y = \pi/2 \pmod{\pi}$, then the transition amplitude becomes zero. For example, let us consider a gap at $k_y = (r/2q)\pi$ with $r = q + 4p$. (We assume that $q \gg p$.) In this case, the minimal value of $|t_r|$ is given by $t_r = 4$, so a naive expectation is that the gap opens in fourth order perturbation. In Fig.5, we illustrate intermediate states. As is seen there, we have to pass through either α_{m-2} or β_{m-2} as an intermediate state, and both of them have

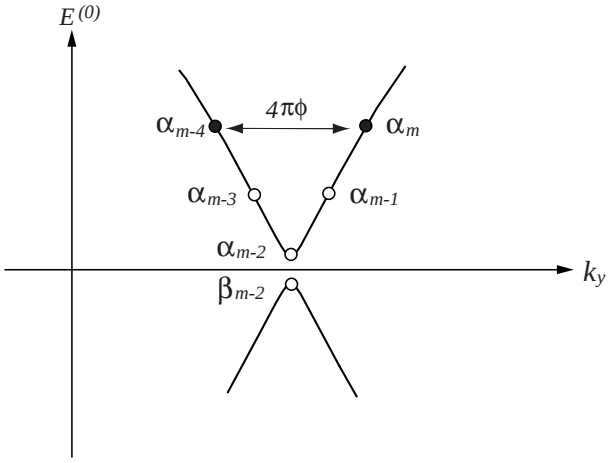

FIG. 5: Intermediate states for a gap at $k_y = (r/2q)\pi$ with $r = q+4p$ in fourth order perturbation. The states α_m and $\alpha_{m'=m-4}$ represented by solid circles are mixed by the perturbation. Open circles represent intermediate states.

$k_y = \pi/2$. From (19) and (21), the transition amplitude to the intermediate state α_{m-2} is proportional to

$$v_+^{(0)}(k_x, k_y^0 + \pi\Phi(m-2)) \propto \Delta^{(0)*}(k_x, \frac{\pi}{2}), \tag{45}$$

and that from β_{m-2} is proportional to

$$u_-^{(0)*}(k_x, k_y^0 + \pi\Phi(m-2)) \propto \Delta^{(0)*}(k_x, \frac{\pi}{2}), \tag{46}$$

and both of them are zero since $\Delta^{(0)}(\boldsymbol{k}) = 0$ at $k_y = \pi/2$. So the matrix element between α_m and α_{m-4} vanishes. As a result, no gap opens in the fourth order perturbation. The gap opens in a higher order perturbation.

Now let us derive a condition that the transition amplitude in $|t_r^0|$th order perturbation vanishes. Without losing generality we can assume that $t_r^0 \neq 0$ since t_r^0 becomes zero only for a gap at $E = 0$, which closes when $\xi \to 0$. We also assume that $|t_r^0| \neq q/2$. The case of $|t_r^0| = q/2$ is discussed later. Consider the mixing between k_y and k_y' with

$$k_y = \left(\frac{r}{2q}\right)\pi, \quad k_y = k_y' + \pi\left(\frac{p}{q}\right)t_r^0, \quad k_y = -k_y' + \pi s_r^0. \tag{47}$$

There are $|t_r^0| - 1$ intermediate states, and since k_x and k_x' are given by

$$k_y = \frac{\pi}{2}s_r^0 + \frac{\pi}{2}\left(\frac{p}{q}\right)t_r^0, \quad k_y' = \frac{\pi}{2}s_r^0 - \frac{\pi}{2}\left(\frac{p}{q}\right)t_r^0, \tag{48}$$

they have momenta

$$k_y'' = \frac{\pi}{2} s_r^0 + \frac{\pi}{2} \left(\frac{p}{q} \right) (t_r^0 - 2l), \tag{49}$$

where

$$l = \begin{cases} 1, 2, \cdots, t_r^0 - 1, & \text{for } t_r^0 > 0, \\ -1, -2, \cdots, t_r^0 + 1, & \text{for } t_r^0 < 0. \end{cases} \tag{50}$$

If k_y'' in (49) becomes $\pi/2$ (mod π), then the transition amplitude in the $|t_r^0|$th order perturbation vanishes. In order for k_y'' to be $\pi/2$ (mod π),

$$\left(\frac{p}{q} \right) (t_r^0 - 2l) \tag{51}$$

must be an integer at least. And to satisfy this $t_r^0 - 2l$ is needed to be a multiple of q since p and q are co-prime integers. But because t_r^0 satisfies

$$|t_r^0 - 2l| \leq |t_r| \leq \frac{q}{2}, \tag{52}$$

this is possible only when $t_r^0 - 2l = 0$. Thus t_r^0 must be even. Furthermore, s_r^0 must be odd in order for k_y'' to be $\pi/2$ (mod π) since $k_y'' = (\pi/2) s_r^0$ when $t_r^0 = 2l$. Therefore only when t_r^0 is an even integer and s_r^0 an odd one, the transition amplitude vanishes. Otherwise, we have a nonzero transition amplitude in the $|t_r^0|$th order perturbation in general.

When t_r^0 is an even integer and s_r^0 an odd one, a nonzero transition amplitude is obtained in the next leading order. The next minimum value of $|t_r|$ is given by

$$t_r = \begin{cases} t_r^0 - q, & \text{for } t_r^0 > 0, \\ t_r^0 + q, & \text{for } t_r^0 < 0. \end{cases} \tag{53}$$

The intermediate states in this order have momenta

$$\begin{aligned} k_y'' &= \frac{\pi}{2} s_r + \frac{\pi}{2} \left(\frac{p}{q} \right) (t_r - 2l) \\ &= \frac{\pi}{2} s_r^0 + \frac{\pi}{2} \left(\frac{p}{q} \right) (t_r^0 - 2l) \end{aligned} \tag{54}$$

with $s_r = s_r^0 + p$ ($s_r = s_r^0 - p$) for $t_r^0 > 0$ ($t_r^0 < 0$) and

$$l = \begin{cases} -1, -2, \cdots, t_r^0 - q + 1, & \text{for } t_r^0 > 0, \\ 1, 2, \cdots, t_r^0 + q - 1, & \text{for } t_r^0 < 0. \end{cases} \tag{55}$$

This k_y'' can not be $\pi/2$ (mod π): In order for k_y'' to be $\pi/2$ (mod π), $t_r^0/2 - l$ must be a multiple of q, but this can not be met from the restriction $0 < |t_r^0/2 - l| < q$.

Now we summarize a procedure to determine the Hall conductance for the rth gap from below under a magnetic field $\Phi = p/q$.

1. First, find a solution of the Diophantine equation, (s_r^0, t_r^0), which satisfies $|t_r^0| \leq q/2$.

2. Then if t_r^0 is an even integer and s_r^0 an odd one, the Hall conductance is given by

$$\sigma_{xy} = \begin{cases} -\frac{e^2}{h}(t_r^0 - q), & \text{for } t_r^0 > 0, \\ -\frac{e^2}{h}(t_r^0 + q), & \text{for } t_r^0 < 0, \end{cases} \tag{56}$$

   The size of the gap is an order $t_a^{q-|t_r^0|}$.

3. For the other cases, the Hall conductance is given by

$$\sigma_{xy} = -\frac{e^2}{h} t_r^0, \tag{57}$$

   and the size of the gap is an order of $t_a^{|t_r^0|}$.

Finally, let us discuss the case of $|t_r^0| = q/2$. This is possible only when q is even and only for gaps with $r = q/2$ or $r = 3q/2$. Although we have two solutions of the Diophantine equation, $t_r^0 = \pm q/2$, the Hall conductance is determined uniquely if $q/2$ is an even integer. Since p is odd when q is even, it can be shown that one of these solutions has an odd s_r^0 and the other has an even s_r^0. So from the argument above, it is found that if $q/2$ is an even number, the solution with an odd s_r^0 has vanishing transition amplitude in the $(q/2)$-th perturbation. Thus the Hall conductance is given by the solution t_r^0 with an even s_r^0.

When $q/2$ is an odd number, both of the solutions with $t_r^0 = \pm q/2$ have non zero transition amplitudes. For $q = 2$, the gap closes since the transition amplitudes of these solutions are the same up to a phase and cancel each other at some k_x, but for the other case, (namely $q = 2(2n + 1)$ with integers n), a gap opens and the Hall conductance is given by t_r^0 with a larger amplitude, which can not be determined algebraically.

C. gap structure and unconventional Hall conductance in a weak magnetic field

Let us now examine the Hall conductance for the weak t_a case in a weak magnetic field. Consider the $r(= qs_r + pt_r)$th gap from the bottom. Since r satisfies $0 < r < 2q$, t_r is

restricted to

$$-\left(\frac{q}{p}\right) s_r < t_r < (2 - s_r)\left(\frac{q}{p}\right). \tag{58}$$

So if $s_r \geq 3$ or $s_r \leq -1$, $|t_r|$ is bounded from below by (q/p). In these cases, the size of the gap $O(t_a^{|t_r|})$ becomes zero in a weak magnetic field limit, $(p/q) \to 0$. Therefore, visible gaps in a weak magnetic field are possible only for the following three classes of r, (a) $r = pt_r$, $(t_r = 1, 2, \cdots,)$, (b) $r = 2q + pt_r$ $(t_r = -1, -2, \cdots,)$, and (c) $r = q + pt_r$ $(t_r = \pm 1, \pm 2, \cdots,)$.

In the case of (a), we have $(s_r^0, t_r^0) = (0, n)$ if we put $t_r = n$ with $0 < n < q/2$. Since s_r^0 is even, the Hall conductance for $r = pn$th gap from below is given by

$$\sigma_{xy} = -\frac{e^2}{h} n, \quad (n = 1, 2, \cdots). \tag{59}$$

Thus the conventional quantization holds in this case. These gaps are near the bottom of the spectrum. In a similar manner, it can be shown that gaps in the class (b) also show the conventional quantization for the Hall conductance. Namely the Hall conductance for the gap with $r = 2q - pn'$ $(0 < n' < q/2)$ is given by

$$\sigma_{xy} = \frac{e^2}{h} n', \quad (n' = 1, 2, \cdots,). \tag{60}$$

These gaps are seen near the top of the spectrum.

For visible gaps in the class (c), we have the unconventional Hall conductance. If we put $t_r = n''$ with $|n''| < q/2$, we have an odd s_r^0. $((s_r^0, t_r^0) = (1, n'').)$ Thus we have a visible gap only if n'' is an odd number, $n'' = 2m + 1$ (m is an integer). Otherwise, the lowest order perturbation is an order of q, then the corresponding gap is invisible in a weak magnetic field limit. For this class of visible gaps with $r = q + p(2m + 1)$ and $|2m + 1| < q/2$, we have the unconventional quantization for the Hall conductance

$$\sigma_{xy} = -\frac{e^2}{h}(2m + 1), \quad (m = 0, \pm 1, \pm 2, \cdots,). \tag{61}$$

These gaps are located around $E = 0$.

IV. STRONG t_a PHASE

Now let us consider the strong coupling limit, $t_a \gg 1$. In this limit, the upper $(E > 0)$ and the lower $(E < 0)$ parts of the spectrum separate from each other, and both of them

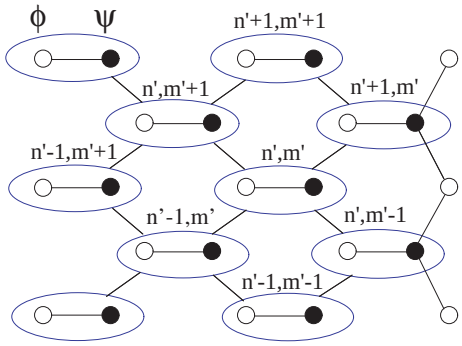

FIG. 6: The square lattice appearing in the strong t_a limit of the honeycomb lattice in Fig.1. Here $n' = (n+m)/2$ and $m' = (m-n)/2$.

are equivalent to that of the square lattice shown in Fig.6. To see this, consider first the case of $\Phi = 0$. When $\Phi = 0$, (11) becomes

$$(h(\boldsymbol{k}) - t_a\sigma_x) \begin{bmatrix} u(\boldsymbol{k}) \\ v(\boldsymbol{k}) \end{bmatrix} = E \begin{bmatrix} u(\boldsymbol{k}) \\ v(\boldsymbol{k}) \end{bmatrix}. \tag{62}$$

In the leading order of the strong coupling limit, this equation reduces to

$$-t_a\sigma_x \begin{bmatrix} u(\boldsymbol{k}) \\ v(\boldsymbol{k}) \end{bmatrix} = E \begin{bmatrix} u(\boldsymbol{k}) \\ v(\boldsymbol{k}) \end{bmatrix}, \tag{63}$$

thus we have two flat bands

$$\frac{1}{\sqrt{2}} \begin{bmatrix} 1 \\ -1 \end{bmatrix}, \quad E = t_a, \tag{64}$$

and

$$\frac{1}{\sqrt{2}} \begin{bmatrix} 1 \\ 1 \end{bmatrix}, \quad E = -t_a. \tag{65}$$

In order to discuss the next leading order, it is convenient to take the following basis,

$$\begin{bmatrix} u(\boldsymbol{k}) \\ v(\boldsymbol{k}) \end{bmatrix} = a(\boldsymbol{k}) \frac{1}{\sqrt{2}} \begin{bmatrix} 1 \\ -1 \end{bmatrix} + b(\boldsymbol{k}) \frac{1}{\sqrt{2}} \begin{bmatrix} 1 \\ 1 \end{bmatrix}. \tag{66}$$

In this basis, (62) is rewritten as

$$\begin{aligned}
&\xi b(\boldsymbol{k}) + \frac{\Delta^{(0)}(\boldsymbol{k}) - \Delta^{(0)*}(\boldsymbol{k})}{2} b(\boldsymbol{k}) - \frac{\Delta^{(0)}(\boldsymbol{k}) + \Delta^{(0)*}(\boldsymbol{k})}{2} a(\boldsymbol{k}) + t_a a(\boldsymbol{k}) = E a(\boldsymbol{k}) \\
&\xi a(\boldsymbol{k}) + \frac{\Delta^{(0)}(\boldsymbol{k}) + \Delta^{(0)*}(\boldsymbol{k})}{2} b(\boldsymbol{k}) - \frac{\Delta^{(0)}(\boldsymbol{k}) - \Delta^{(0)*}(\boldsymbol{k})}{2} a(\boldsymbol{k}) - t_a b(\boldsymbol{k}) = E b(\boldsymbol{k}),
\end{aligned} \tag{67}$$

and we can neglect the mixing terms between the upper band and lower one in the next leading order. Therefore, we have

$$\begin{aligned}
&- \frac{\Delta^{(0)}(\boldsymbol{k}) + \Delta^{(0)*}(\boldsymbol{k})}{2} a(\boldsymbol{k}) + t_a a(\boldsymbol{k}) = E a(\boldsymbol{k}), \\
&\frac{\Delta^{(0)}(\boldsymbol{k}) + \Delta^{(0)}(\boldsymbol{k})}{2} b(\boldsymbol{k}) - t_a b(\boldsymbol{k}) = E b(\boldsymbol{k}).
\end{aligned} \tag{68}$$

The eigen energies of these equations are $E = \pm(t_a + 2\cos k_x \cos k_y)$. By changing variables as $k_1' = k_x + k_y$ and $k_2' = k_y - k_x$, they reduce to the energies of a pair of the tight binding models on the square lattice up to the constant shifts $\pm t_a$,

$$E = \pm(t_a + \cos k_1' + \cos k_2'). \tag{69}$$

Now consider the case of $\Phi = p/q$. For this purpose, we take a new gauge for the magnetic field and consider the following equations,

$$\begin{aligned}
&- e^{i\pi\Phi(n+m)} \phi_{n+1,m-1} - \phi_{n+1,m+1} - t_a \phi_{n,m} + \xi \psi_{n,m} = E \psi_{n,m}, \\
&-e^{-i\pi\Phi(n+m)} \psi_{n-1,m+1} - \psi_{n-1,m-1} - t_a \psi_{n,m} - \xi \phi_{n,m} = E \phi_{n,m}.
\end{aligned} \tag{70}$$

In terms of $a(\boldsymbol{k})$ and $b(\boldsymbol{k})$, these equations are rewritten as

$$\begin{aligned}
&-\frac{e^{-ik_2'}}{2} \left(b(k_1' - 2\pi\Phi, k_2') - a(k_1' - 2\pi\Phi, k_2')\right) + \frac{e^{ik_2'}}{2} \left(b(k_1' + 2\pi\Phi, k_2') + a(k_1' + 2\pi\Phi, k_2')\right) \\
&+ \cos k_1' a(\boldsymbol{k}') - i \sin k_1' b(\boldsymbol{k}') + t_a a(\boldsymbol{k}') + \xi b(\boldsymbol{k}') = E a(\boldsymbol{k}'), \\
&-\frac{e^{-ik_2'}}{2} \left(b(k_1' - 2\pi\Phi, k_2') - a(k_1' - 2\pi\Phi, k_2')\right) - \frac{e^{ik_2'}}{2} \left(b(k_1' + 2\pi\Phi, k_2') + a(k_1' + 2\pi\Phi, k_2')\right) \\
&- \cos k_1' b(\boldsymbol{k}') + i \sin k_1' a(\boldsymbol{k}') - t_a b(\boldsymbol{k}') + \xi a(\boldsymbol{k}') = E b(\boldsymbol{k}'),
\end{aligned} \tag{71}$$

where (k_1', k_2') are momentum conjugate to the coordinate (n', m'), which are given by $k_1' = k_x + k_y$ and $k_2' = k_y - k_x$. In the leading order, we have again the two flat bands,

$$t_a a(\boldsymbol{k}') = E a(\boldsymbol{k}'), \quad -t_a b(\boldsymbol{k}') = E b(\boldsymbol{k}'), \tag{72}$$

and in the next leading order, the mixing terms between the upper band ($E = t_a$) and lower one ($E = -t_a$) can be neglected as

$$\frac{e^{ik_2'}}{2}a(k_1' + 2\pi\Phi, k_2') + \frac{e^{-k_2'}}{2}a(k_1' - 2\pi\Phi, k_2') + \cos k_1 a(\boldsymbol{k}') = (E - t_a)a(\boldsymbol{k}'),$$
$$-\frac{e^{ik_2'}}{2}b(k_1' + 2\pi\Phi, k_2') - \frac{e^{-ik_2'}}{2}b(k_1' - 2\pi\Phi, k_2') - \cos k_1' b(\boldsymbol{k}') = (E + t_a)b(\boldsymbol{k}'). \tag{73}$$

These equations coincide with that of the tight-binding model on the square lattice illustrated in Fig.6 except for the constant shift in the energies.

Using the results of the tight binding models on the square lattice in [16, 22], we can determine the Hall conductance for r-th gap in the strong t_a limit as

$$\sigma_{xy} = -\frac{e^2}{h}t_r^0, \tag{74}$$

where t_r^0 is a solution of the Diophantine equation with $|t_r^0| \leq q/2$. For $r = q/2$ and $r = 3q/2$, we can not determine the Hall conductance algebraically since we have two solutions $t_r^0 = \pm q/2$. The corresponding gaps in the strong coupling limit close, but for a strong but finite t_a they open from a mixing between the upper band and the lower one. The Hall conductance is given by one of the two possible values of $t_a(= \pm q/2)$, but there is no algebraic rule to determine it.

Let us comment briefly the Hall conductance for the strong t_a case in a weak magnetic field. As was shown before, only three classes of gaps are visible in a weak magnetic field: (a) $r = pt_r$, $(t_r = 1, 2, \cdots,)$, (b) $r = 2q + pt_r$, $(t_r = -1, -2, \cdots,)$, (c) $r = q + pt_r$, $(t_r = \pm 1, \pm 2, \cdots,)$. For these classes of gaps, we have (a) $(s_r^0, t_r^0) = (0, n)$ $(0 < n < q/2)$, (b) $(s_r^0, t_r^0) = (2, -n')$ $(0 < n' < q/2)$ and (c) $(s_r^0, t_r^0) = (1, n'')$ $(|n''| < q/2)$, respectively. In contrast to the weak t_a case, the formula (74) indicates that all of them show the conventionally quantized Hall conductance.

V. PHASE TRANSITIONS IN INTERMEDIATE t_a REGION

A. topological quantum phase transitions

In the above we have calculated the Hall conductance in two opposite limits, $t_a \to 0$ and $t_a \to \infty$. The algebraic rules to determine the Hall conductances in the both limits were given and it was found that for gaps with even t_r^0 and odd s_r^0 the Hall conductances take

different values from each other. It implies that each gap in this class closes at some t_a at least once in order to change the corresponding topological number t_r. In other words, we should have a quantum phase transition between topological insulator phases at some t_a if the Fermi energy is located in a gap in this class.

In the following, we will confirm the existence of the quantum phase transition numerically. In addition, we will find that an unexpected topological quantum phase transition occurs due to the van Hove singularity.

B. numerical studies of quantum phase transitions

Here, we will study the whole region of t_a for a number of cases of $\Phi = p/q$ by using numerical calculations. We will find that except for a few gaps either the strong t_a limit or the weak t_a one explains the gap structures qualitatively and the Hall conductance quantitatively: For a weak t_a region, $0 < t_a \leq 1$, the gap structures are the same as those in the weak t_a limit, and for a strong t_a region, $t_a > 2$, they are the same as those in the strong t_a limit. In the intermediate region, $1 < t_a \lesssim 2$, we have the topological quantum phase transitions mentioned in the previous subsection and the gap structure changes from those in the weak t_a region to those in the strong one. From the topological nature of the Hall conductance, these results imply that except for a few gaps the Hall conductances in the whole t_a region are determined algebraically by using either those in the weak t_a region or those in the strong one.

It will be shown that the exceptional gaps appear just beyond the van Hove singularity at $t_a = 1$ (namely the van Hove singularity in graphene) or on the lower and the upper edges of the spectrum. For some gaps in these regions, additional topological quantum phase transitions, which are unexpected from the analysis in the two limits, are observed. It will be found that multiple topological quantum phase transitions occur for these gaps.

In the following we limit our calculation to $0 \leq \Phi \leq 1/2$ without losing generality: This is because the spectrum is invariant under translation $\Phi \to \Phi + n$ with an integer n, and reflection about half integer values of Φ. Furthermore a close inspection of the model also shows that the spectrum is unchanged under reflection $E \leftrightarrow -E$ for a given $\Phi = p/q$.

We illustrate typical examples of energy spectra in Figs.7-13. For $\Phi = 1/2, 1/3$ and $1/4$, as is shown in Fig.7, none of the gaps closes in a finite region of t_a, and a gap opens at

$E = 0$ when $t_a > 1$. Since the Hall conductances for the unclosed gaps remain the same values when t_a changes, they can be calculated algebraically by using the results of the weak t_a limit or those of the strong one. The Hall conductances determined in this manner are also shown in Fig.7. For some gaps, both the weak and strong t_a analyses can be used to determine the Hall conductances and they are found to give consistently the same values.

For $\Phi = 1/5$ and $2/5$, there are gap closing points in the energy spectra at $t_a \sim 2$. See Figs.8 and 9. It is found that for the gaps with the gap closing points, the Hall conductances obtained in the weak t_a analysis are different from those in the strong one. This means that the gap closing points are required by the topological quantum phase transition described in Sec.V A. In Figs.8 and 9 we also illustrate intermediate states in the weak t_a perturbation. One can see that for the gaps with the gap closing points, there exists the intermediate state with $k_y = \pm\pi/2$ (mod. π). For the other gaps we have no intermediate states with the these momenta. Similar gap closing points are also found for $\Phi = 1/6, 1/7, 2/7$ and $3/7$ in Fig.10. These gap closing points are also required by the topological quantum phase transition. It is shown in Fig.10 how t_r of the Hall conductance $\sigma_{xy} = -(e^2/h)t_r$ changes from the weak t_a region to the strong one.

When q is large ($q \geq 7$), a new kind of gap closing points, which are not required by the topological difference between the weak and strong t_a limits, appears for some exceptional gaps. For example, see Fig. 12. We have two gap closing points in the same gap where the quantum Hall conductance in the weak t_a limit is the same as that in the strong t_a limit. There is no a prior topological reason why the gap should close in the intermediate t_a. The possible origin of the additional gap closing points is accumulation of gaps at these singularities. For a large q, many magnetic bands are accumulated both near the van Hove singularity at $t_a = 1$ and on the lower and upper edges of the spectrum, so the gaps near the singularities become narrow and are easy to close as the accumulation grows. Except near the singularities, we did not observe the additional gap closing points

To illustrate the weak magnetic field case, $\Phi \ll 1$, we also show the energy spectra for $1/25$, $1/40$ and $1/50$ in Figs.11, 12 and 13. The Hall conductances for visible gaps are also shown in these figures. It is found that in the weak t_a region including the graphene case ($t_a = 1$) the Hall conductances are unconventionally quantized as $\sigma_{xy} = e^2(2n+1)/h$, ($n = 0, \pm1, \pm2, \cdots$) near half-filling ($E = 0$), while in the strong t_a region they are conventionally quantized as $\sigma_{xy} = e^2 n/h$, ($n = 0, \pm1, \pm2, \cdots$).

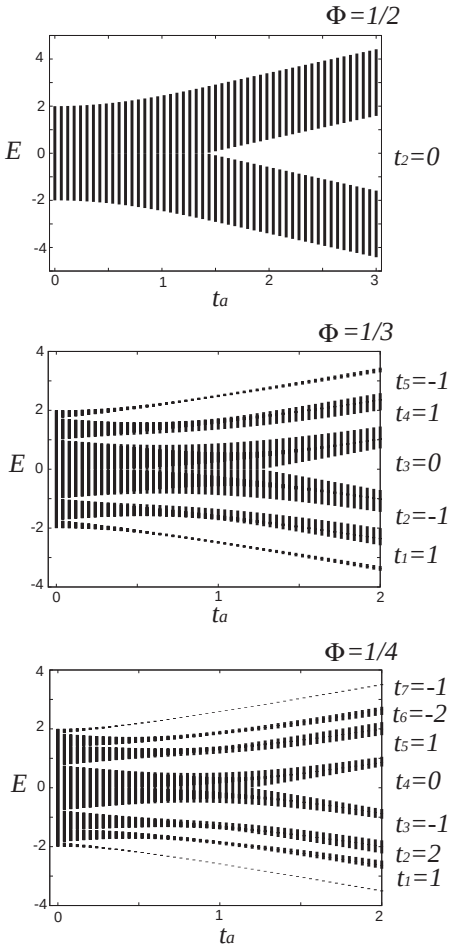

FIG. 7: The energy spectra v.s t_a for $\Phi = 1/2$, $1/3$, and $1/4$. None of gaps closes as we make t_a stronger. The Hall conductance $\sigma_{xy} = -(e^2/h)t_r$ for r-th gap from the bottom, which is calculated algebraically by the method described in the text, is also shown.

VI. GRAPHENE CASE ($t_a = 1$)

A. Hall conductance

Let us now apply our results to graphene, where t_a is given by 1, and determine its Hall conductances. As was shown in Sec.V B, the numerical studies strongly suggest that for most energy regions graphene ($t_a = 1$) is in the weak t_a phase: Except the energy regions just beyond the van Hove singularities at $E = \pm 1$ (namely, the energy regions where $|E|$ is slightly greater than 1) or those on the lower and upper edges of the spectrum none of gaps closes as we change t_a from 0 to 1, and the structure of the energy spectrum is qualitatively

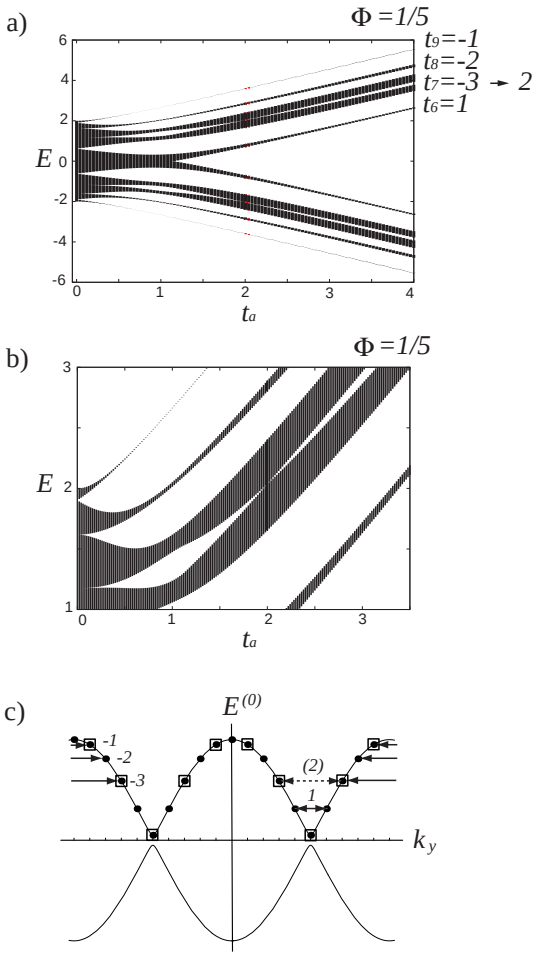

FIG. 8: a) The energy spectrum for $\Phi = 1/5$. b) A closer look at the gap closing point in the seventh gap from the bottom. c) The unperturbed states and the mixing in the weak t_a perturbation for $\Phi = 1/5$. The states with the same symbol are related to each other in the perturbation. The solid arrows indicate the mixing between states. The dotted arrow indicates the mixing with vanishing amplitude, which has an intermediate state with the singular momentum $k_y = \pi/2$. Integers denote t_r for the mixing.

the same as that in the weak t_a limit. In particular, if we consider the r-th gap from the bottom, only the gaps with the following three classes of r are visible in a weak magnetic field: (a) $r = pt_r$, $(t_r = 1, 2, \cdots,)$, (b) $r = 2q + pt_r$, $(t_r = -1, -2, \cdots,)$ (c) $r = q + pt_r$, $(t_r = \pm 1, \pm 3, \pm 5, \cdots,)$.

These results indicates that even when $t_a = 1$ the perturbation theory works well at least qualitatively for gaps away from the exceptional energy regions. From the topological

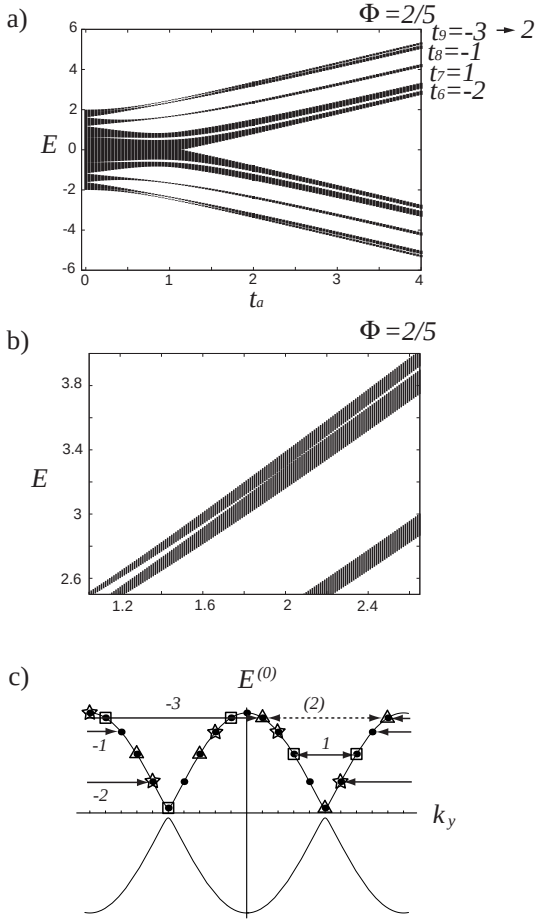

FIG. 9: a) The energy spectrum v.s t_a for $\Phi = 2/5$. b) A closer look at the gap closing point in the ninth gap from the bottom. c) The unperturbed states and the mixing in the weak t_a perturbation for $\Phi = 2/5$.

nature of the Hall conductance, it implies that the Hall conductances in graphene for these gaps are quantitatively the same as those at the weak t_a limit. Namely they are determined algebraically by the rule (56) and (57). In addition to the visible gaps in a weak magnetic field, this rule also determines the Hall conductances for the subband gaps in a strong magnetic field.

This result consistently explains the unconventional quantization of the Hall conductance observed experimentally near half filling [1, 2]. Among the visible gaps in a weak magnetic field, only those in the class (c) include the gaps near half filling ($E = 0$). They show the unconventional quantization of the Hall conductance, $\sigma_{xy} = -e^2 t_r/h$ ($t_r = \pm 1, \pm 3, \cdots,$).

We emphasize here that our result indicates the unconventional Hall conductance persists

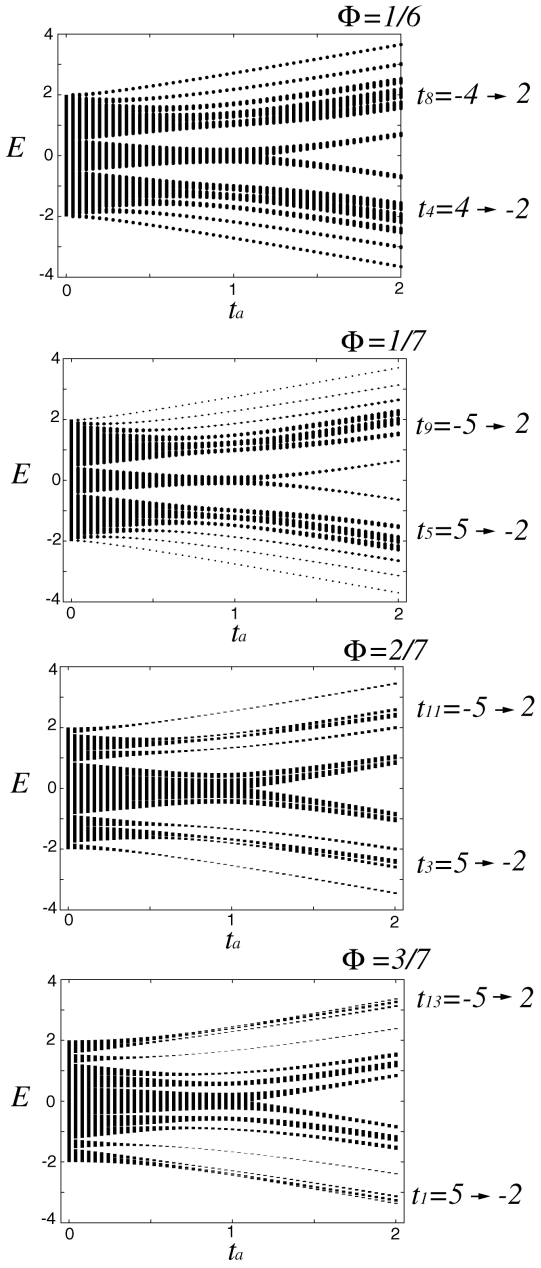

FIG. 10: The energy spectra v.s t_a for $\Phi = 1/6$, $1/7$, $2/7$ and $3/7$. The gap closing points appear whenever the Hall conductance ($\sigma_{xy} = -(e^2/h)t_r$) in the weak t_a region is different from that in the strong t_a region.

up to the van Hove singularities, where the Dirac fermion description is no longer valid. This is because none of gaps in this energy region closes when we change t_a from 0 to 1. They are well described by the weak t_a analysis and the Hall conductance for the visible gaps in a weak magnetic field shows the unconventional quantization. (Note that they belongs

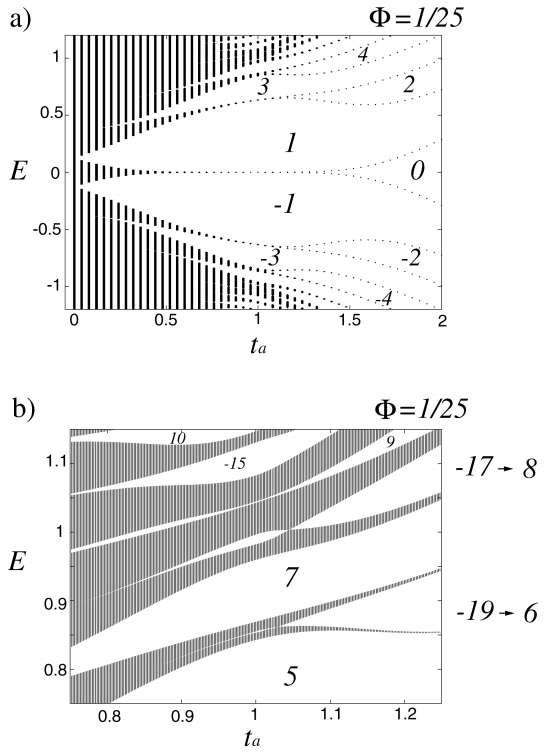

FIG. 11: a) The energy spectrum v.s t_a for $\phi = 1/25$. Integers in the gaps indicates t_r of the Hall conductance $\sigma_{xy} = -(e^2/h)t_r$. b) A closer look at gap closing points near $t_a = 1$. It is found that gap closing points appear only when $t_a > 1$. The gap with $t_r = -15$ closes at $t_a \sim 1.25$ (not shown).

to the class (c) above.) This anomalous behavior of the Hall conductance on honeycomb lattice was already reported in a numerical calculation [8], but our study here establishes this analytically. Furthermore, at the same time, it reveals why the unconventional Hall conductance does not persist beyond the van Hove singularities: For gaps just beyond the van Hove singularities, a gap closing point can appear when t_a changes from 0 to 1. So in general the weak t_a analysis does not apply to the gaps in this region and there is no reason why the unconventional Hall conductances hold. The unconventional quantization of the Hall conductance up the the van Hove singularities should be observed if the chemical potential can be varied over a wide range in graphene.

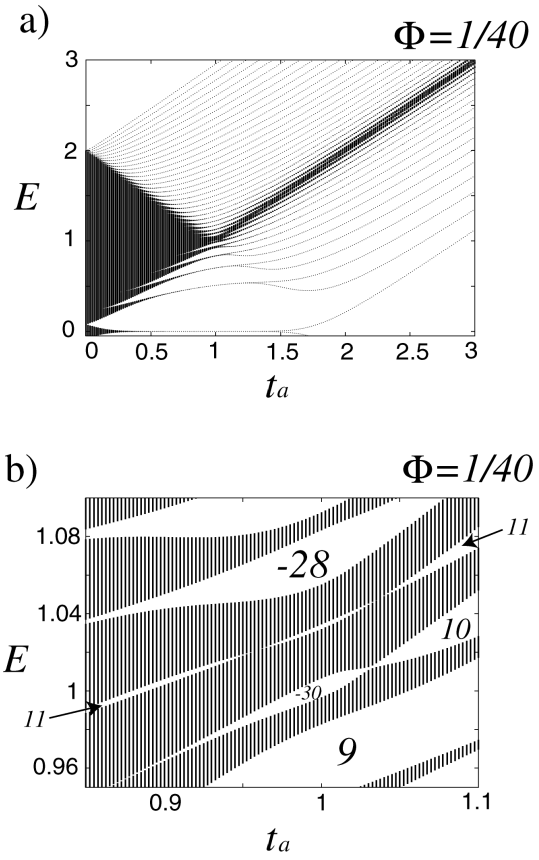

FIG. 12: a) The energy spectrum v.s t_a for $\phi = 1/40$. b) A closer look at gap closing points near $t_a = 1$. Integers in the gaps indicate t_r of the Hall conductance $\sigma_{xy} = -(e^2/h)t_r$. For the gap with $t_r^0 = 11$, we have two gap closing points which are not required by the topological difference between the weak and strong t_a limits.

B. edge states

To confirm the results in the previous section, we compare here the bulk quantum Hall conductance obtained by the rule (56) and (57) and the number of edge states obtained numerically for finite systems with $t_a = 1$. From the bulk-edge correspondence in quantum Hall systems [23, 24, 25, 26], these quantum numbers should coincide with each other for gaps with no gap closing point in the region $0 < t_a \leq 1$. In other words, the results in the previous section suggest that they should be the same except for some gaps just beyond the van Hove singularities or those on the upper and lower edges in the spectrum.

To calculate the number of edge states, we consider cylindrical systems with bearded

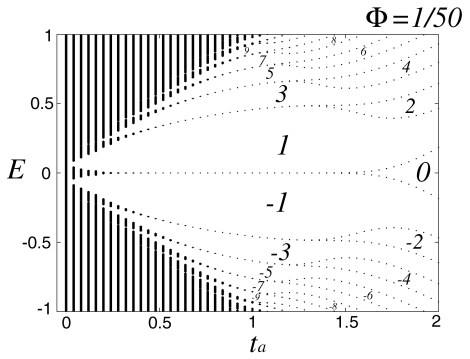

FIG. 13: The energy spectrum v.s. t_a for $\phi = 1/50$. Integers indicate t_r of the Hall conductance $\sigma_{xy} = -(e^2/h)t_r$.

edges at both ends. For all possible $\Phi = p/q$ ($0 < \Phi \leq 1/2$) with $1 \leq q \leq 11$, the energy spectra of these systems are obtained numerically and the numbers of the edge states are evaluated. We also examine the case of $\Phi = 1/25$ as a weak magnetic field case.

In Fig.14, we illustrate the energy spectra for $5 \leq q \leq 7$. Except for gaps near the singularities mentioned above, we have excellent agreements between the number of the edge states and the bulk Hall conductance determined by the rule (56) and (57). In particular, even for the subband gaps, which become invisible in a weak magnetic field, these two quantum numbers are found to agree with each other. This results clearly indicate that except for gaps near the singularities, the Hall conductances in graphene including those for subband gaps are determined by the rule (56) and (57). In addition, for some gaps located just beyond the van Hove singularity at $E = 1$ or those on the lower and upper edges of the spectra, we find a disagreement between them, which is also consistent with the analyses presented in the previous section. We also checked that the similar results hold for all $\Phi = p/q$ with $q \leq 11$. We summarize the results for the bulk Hall conductance and the edge Hall conductance in Tables I and II.

To illustrate a weak magnetic field case, the energy spectrum with bearded edges for $\Phi = 1/25$ is also shown in Fig.15. In a weak magnetic field, subband gaps are very tiny so only the edge states for visible gaps are shown in the figure. The unconventional quantization for the edge quantum Hall conductance is found to persist up the van Hove singularities at $E = \pm 1$. We also find that for gaps beyond the van Hove singularities the conventional

a) $\Phi = 1/5$

r	(s_r^0, t_r^0)	$\sigma_{xy}^{\rm weak}$	$\sigma_{xy}^{\rm edge}$
1	(0,1)	1	1
2	(0,2)	2	2
3	(1,-2)	3	3
4	(1,-1)	-1	-1

b) $\Phi = 2/5$

r	(s_r^0, t_r^0)	$\sigma_{xy}^{\rm weak}$	$\sigma_{xy}^{\rm edge}$
1	(1,-2)	3	3
2	(0,1)	1	1
3	(1,-1)	-1	-1
4	(0,2)	2	2

c) $\Phi = 1/6$

r	(s_r^0, t_r^0)	$\sigma_{xy}^{\rm weak}$	$\sigma_{xy}^{\rm edge}$
1	(0,1)	1	1
2	(0,2)	2	2
3	(0,3) or (1,-3)	3 or -3	3
4	(1,-2)	4	4
5	(1,-1)	-1	-1

d) $\Phi = 1/7$

r	(s_r^0, t_r^0)	$\sigma_{xy}^{\rm weak}$	$\sigma_{xy}^{\rm edge}$
1	(0,1)	1	1
2	(0,2)	2	2
3	(0,3)	3	3
4	(1,-3)	-3	4
5	(1,-2)	5	5
6	(1,-1)	1	1

e) $\Phi = 2/7$

r	(s_r^0, t_r^0)	$\sigma_{xy}^{\rm weak}$	$\sigma_{xy}^{\rm edge}$
1	(1,-3)	-3	-3
2	(0,1)	1	1
3	(1,-2)	5	5
4	(0,2)	2	2
5	(1,-1)	-1	-1
6	(0,3)	3	3

f) $\Phi = 3/7$

r	(s_r^0, t_r^0)	$\sigma_{xy}^{\rm weak}$	$\sigma_{xy}^{\rm edge}$
1	(1,-2)	5	5
2	(-1,3)	3	3
3	(0,1)	1	1
4	(1,-1)	-1	-1
5	(2,-3)	-3	-3
6	(0,2)	2	2

TABLE I: The bulk Hall conductance $\sigma_{xy}^{\rm weak}$ (in units of $-(e^2/h)$) of r-th gap from the bottom determined by (56) and (57), and the corresponding edge Hall conductance $\sigma_{xy}^{\rm edge}$ determined by counting the edge states for a) $\Phi = 1/5$, b) $\Phi = 2/5$, c) $\Phi = 1/6$, d) $\Phi = 1/7$, e) $\Phi = 2/7$ and f) $\Phi = 3/7$. The edge states are counted for $t_a = 1$. We also show the solution of the Diophantine equation (s_r^0, t_r^0) satisfying $|t_r^0| \leq q/2$. Here we have shown $\sigma_{xy}^{\rm weak}$ and $\sigma_{xy}^{\rm edge}$ for gaps in the lower band ($E < 0$) since those for the $(2q - r)$th gap in the upper band are the same as those for rth gap in the lower band with opposite signs.

quantization for the edge quantum Hall conductance holds. The latter result suggests that the rule (56) and (57) is no longer valid for some visible gaps located just beyond the van Have singularities. These results are also consistent with those in the previous section.

Φ	r	(s_r^0, t_r^0)	$\sigma_{xy}^{\rm weak}$	$\sigma_{xy}^{\rm edge}$
1/7	4	(1,-3)	3	-4
	10	(1,3)	-3	4
1/8	5	(1,-3)	3	-5
	11	(1,3)	-3	5
1/9	6	(1,-3)	3	-6
	12	(1,3)	-3	6
4/9	2	(2,-4)	4	-5
	16	(0,4)	-4	5
1/11	6	(1,-5)	5	-6
	16	(1,5)	-5	6
5/11	2	(2,-4)	4	-7
	20	(0,4)	-4	7

TABLE II: A list of gaps where $\sigma_{xy}^{\rm edge}$ disagrees with $\sigma_{xy}^{\rm weeak}$ ($q \leq 11$) . The edge states are counted for $t_a = 1$. For $\Phi = 4/9$ and $\Phi = 5/11$, the gaps are located on the lower and upper edges of the spectra, and for the other cases, they are located just beyond the van Hove singularity. All of them are located at $|E| > 1$.

VII. CONCLUSION

In this paper, we examined quantum phase structures of a tight-binding model on the honeycomb lattice, which are controlled by the hopping parameter t_a. In contrast to the square lattice, where no phase transition occurs by changing the ratio of hopping parameters t_x/t_y, it was found that phase transitions occur as we change t_a. In terms of the Diophantine equation, we characterized the weak t_a phase and the strong t_a one, respectively, and determined the Hall conductances for both cases. We found that the weak t_a phase shows the unconventional quantization of the Hall conductance in a weak magnetic field although the strong t_a phase shows only the conventional one. This implies the existence of quantum phase transitions accompanying gap closing points in the intermediate t_a region, which was confirmed by numerical calculations. We also found numerically that unexpected quantum

phase transitions occur for some gaps just beyond the van Hove singularities at $t_a = 1$ or those on the upper and lower edges of the spectrum.

Using these results, we analyzed in detail the Hall conductance in graphene ($t_a = 1$). Except for some gaps just beyond the van Hove singularities or on the edges of the spectrum, the Hall conductances including those for the subband gaps were determined. They naturally explain the experimentally observed unconventional quantization of the quantum Hall effect in a weak magnetic field. They also predict that the unconventional quantization persists up to the van Hove singularity. We also examined the edge states in graphene and confirmed the bulk-edge correspondence in quantum Hall effect.

[1] K. S. Novoselov, E. McCann, S. V. Morozov, V. I. Fal'ko, M. I. Katsnelson, V. Zeitler, D. Jiang, F. Schedin, and A. K. Gein, Nature **438**, 197 (2005).

[2] Y. Zhang, Y. W. Tan, H. L. Stormer, and P. Kim, Nature **438**, 201 (2005).

[3] V. P. Gusynin and S. G. Sharapov, Phys. Rev. Lett. **95**, 146801 (2005).

[4] Y. Zheng and T. Ando, Phys. Rev. B **65**, 245420 (2002).

[5] N. M. R. Peres, F. Guinea, and A. H. C. Neto, Phys. Rev. B **73**, 125411 (2006).

[6] K. S. Novoselov, E. McCann, S. V. Morozov, V. I. Fal'ko, M. I. Katsnelson, U. Zeitler, D. Jiang, F. Schedin, and A. K. Geim, Nat. Phys. **2**, 177 (2006).

[7] M. Oshikawa, Phys. Rev. B **50**, 17357 (1994).

[8] Y. Hatsugai, T. Fukui, and H. Aoki, Phys. Rev. B **74**, 205414 (2006).

[9] R. Rammal, J. Phy. (Paris) **46**, 1345 (1985).

[10] Y. Hasegawa and M. Kohmoto, Phys. Rev. B **74**, 155415 (2006).

[11] B. A. Bernevig, T. L. Hughes, S. C. Zhang, H. D. Chen, and C. Wu, Int. J. Mod. Phys. B **20**, 3257 (2006).

[12] Y. Hasegawa, R. Konno, H. Nakano, and M. Kohmoto, Phys. Rev. B **74**, 033413 (2006).

[13] P. Dietl, F. Piéchon, and G. Montambaux, Phys. Rev. Lett. **100**, 236405 (2008).

[14] A. H. MacDonald, Phys. Rev. B **29**, 3057 (1984).

[15] S. Aubry and G. André, Ann. Isr. Phys. Soc. **3**, 133 (1980).

[16] D. J. Thouless, M. Kohmoto, M. P. Nightingale, and M. den Nijs, Phys. Rev. Lett. **49**, 405 (1982).

[17] M. Kohmoto, J. Phys. Soc. Jpn. **61**, 2645 (1992).

[18] P. Středa, J. Phys. C **15**, L717 (1982).

[19] P. Středa, J. Phys. C **15**, L1299 (1982).

[20] M. Kohmoto, Ann, Phys. (N.Y.) **160**, 343 (1985).

[21] J. E. Avron, R. Seiler, and B. Simon, Phys. Rev. Lett. **51**, 51 (1983).

[22] M. Kohmoto, Phys. Rev. B **39**, 11943 (1988).

[23] B. I. Halperin, Phys. Rev. B **25**, 2185 (1982).

[24] Y. Hatsugai, Phys. Rev. B **48**, 11851 (1993).

[25] Y. Hatsugai, Phys. Rev. Lett. **71**, 3697 (1993).

[26] X.-L. Qi, Y.-S. Wu, and S.-C. Zhang, Phys. Rev. B **74**, 085308 (2006).

[27] Y. Zhang, Z. Jiang, M. S. Purewal, Y. W. Tan, M. Fazlollahi, J. D. Chudow, J. A. Jaszczak, H. L. Stormer, and P. Kim, Phys. Rev. Lett. **96**, 136806 (2006).

[28] Z. Jiang, Y. Zhang, H. L. Stormer, and P. Kim, Phys. Rev. Lett. **99**, 106802 (2007).

[29] Recent experimental studies revealed new quantum Hall states which is not included in (1) [27, 28]. The electron-electron interaction presumably plays a crucial role for them.

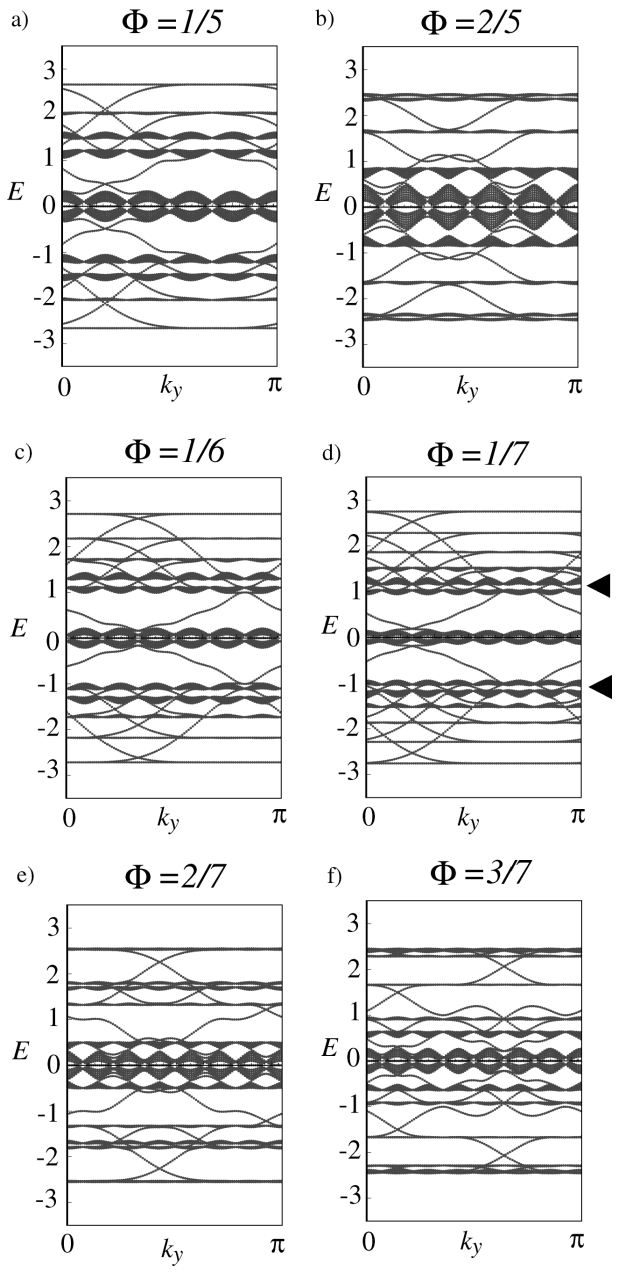

FIG. 14: The energy spectra of graphene (honeycomb lattice with $t_a = 1$) with bearded edges for a) $\Phi = 1/5$, b) $\Phi = 2/5$, c) $\Phi = 1/6$, d) $\Phi = 1/7$, e) $\Phi = 2/7$ and d) $\Phi = 3/7$. Here k_y denotes the momentum along the edges. Edge states are seen in the energy gaps in the spectra. The arrows in d) indicate gaps where the number of edge states disagrees with the Hall conductance obtained by (56) and (57). Except these gaps, we have agreements between the numbers of edge states and the bulk Hall conductances determined by (56) and (57).

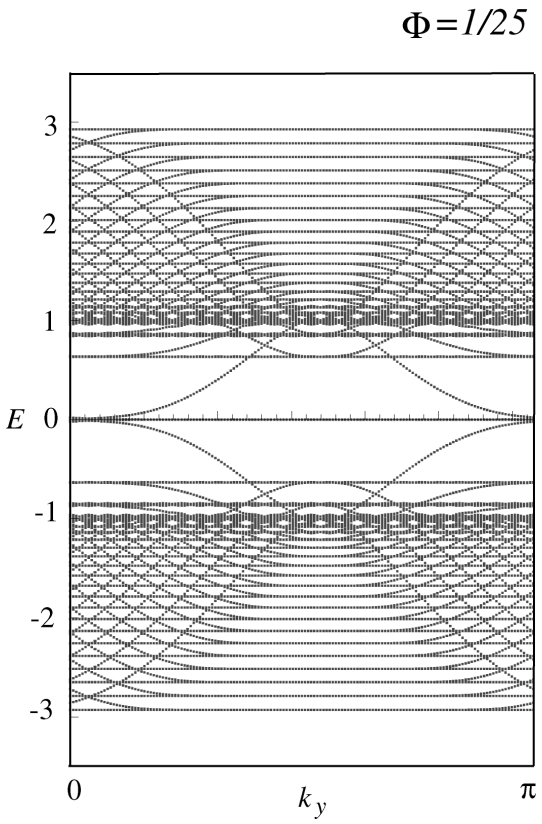

FIG. 15: The energy spectrum of graphene with bearded edges for $\Phi = 1/25$. Here k_y is the momentum along the edges. By counting edge states, we have $\sigma_{xy}^{\rm edge} = -(e^2/h)(2n+1)$ with $n = -2, -1, 0, 1$ near $E = 0$. For the other regions, we have the conventional quantization of the Hall conductance.